Broadband polarization beam splitter based on a negative refractive lithium niobate photonic crystal slab

Siqi Duan (段斯琪), Yuping Chen (陈玉萍)*, Guangzhen Li (李广珍), Chuanyi Zhu (朱传义), and Xianfeng Chen (陈险峰)

Department of Physics and Astronomy, Shanghai Jiao Tong University, State Key Laboratory of Advanced Optical Communication Systems and Networks, Shanghai 200240, China

**Corresponding author: ypchen@sjtu.edu.cn*

Received December 9, 2015; accepted February 4, 2016; posted online March 16, 2016

Using a lithium niobate (LN) material, we propose a broadband polarization beam splitter (PBS) with high efficiency by employing a negative refractive photonic crystal (PhC) wedge slab with an angle of 60°. It can split the incident light into two parts at about 90° with TE and TM polarizations. The transmissions of polarized light for an LN-based PBS are more than 80% with a broad angle and wavelength bandwidth of 8° and 70 nm at 1.55 μm, while with a Si-based PhC, no PBS with high efficiency can be realized for the relatively lower transmission of TM output light.

OCIS codes: 230.5298, 230.3120, 130.3730.
doi: 10.3788/COL201614.042301.

The polarization beam splitter (PBS) can split two different beams of mutually orthogonal polarizations along different directions. The PBS has played an important role in optical fiber communication and integrated optics as an important device in polarization optical correlation systems. The traditional PBS[1,2] uses birefringence in a natural crystal or polarization selectivity in a multiplayer structure to realize polarization splitting based on the Brewster angle. But it has the following drawbacks: (1) the natural crystal requires a high thickness, (2) the multilayer structure has a complex processing technology with a millimeter level size that cannot be applied to the micro-machining technology, (3) it is sensitive to the change of angle, and (4) the transmission light has a low extinction ratio. Therefore, the traditional PBS cannot meet the size needs of modern integrated optics systems.

In recent years, several kinds of PBSs[3–5] based on photonic crystals (PhCs)[6–8] have been developed. The main characteristic of a PhC is its photonic bandgap (PBG), which forbids the propagation of photons in a certain range of frequencies[9–11]. One kind of PBS is used for the effective refractive index of the PhC, which is +1 for TE polarization and −1 for TM polarization[12]. It has a small angle and wavelength bandwidth. Due to the large boundary reflection of TM polarization, the PBS has low light transmission, which results in an incomplete separation between TE and TM polarizations. Another kind of PBS is used for the spectral shift in the lowest PBG for TE polarization and TM polarization[13,14]. It is difficult to obtain large extinction ratios because of the non-negligible reflection. For a Si-based PhC PBS, one can also use a self-collimating PhC[15].

Recently, more research has been focused on lithium niobate (LN)-based PhCs[16–18], since LN[19] is called "optical silicon" for an integrated optical system. It is an important nonlinear optical material[20] with a wide transmission spectral width (400 nm to 5.5 μm), and has more applications in achieving wavelength converters[21], optical logic gates and computers[22,23], etc., and especially in generating quantum polarization sources by spontaneous parametric down conversion (SPDC)[24]. It is well known that the conventional PBS is generally used to obtain quantum polarization entanglement sources combined with SPDC, but it can be used in free space. So an on-chip lab-scaled LN-based PBS is critically required for quantum-integrated optical sources.

In this Letter, we propose an LN-based PBS by using a refractive negative PhC slab that features two different PBGs and the propagation conditions of TE polarization and TM polarization at the wavelength of 1.55 μm. This pillar-type wedge PhC slab has a lattice constant of 0.816 μm and a rod radius of 244.8 nm. This PBS can separate the incident light with TE:TM = 1:1 and has a high polarization extinction ratio and transmission within a certain angle and wavelength ranges, which means it has the characteristic of tunability. When the transmission is over 80%, the angle bandwidth and wavelength bandwidth for LN-based PBS are 8° and 70 nm, a transmission no Si-based PBS can achieve.

Here, we demonstrate a PBS based on negative refraction. The principle of negative refraction is shown in Fig. 1(a). The circle represents the equi-frequency contour line. The frequency decreases from the inner ring to the outer ring for the PhC and increases for the air. The direction of the group velocity $Vg = \partial\omega/\partial k$ is along the increasing direction of the contour line. Therefore, the wave vector k and group velocity Vg are in the same direction in the air. In the PhC, k and Vg are in the opposite directions. The wave vector k is on the same side of the normal at the interface of the air and the PhC, which results in negative refraction.

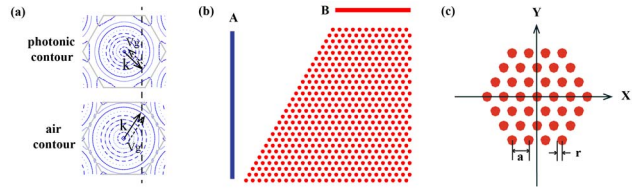

Fig. 1. Configuration of the negative refractive PhC. (a) The principle of negative refraction. The direction of group velocity is along the increasing direction of the contour line. The wave vector is on the same side of the normal at the interface of the air and the PhC. (b) The two-dimensional PhC based on LN. Ports A and B are the two receivers to measure the transmission of the incident light. (c) The enlarged structure of the PhC with a hexagonal array. a is the lattice constant. r is the radius of the dielectric rod.

The negative refractive PhC we constructed is shown in Figs. 1(b) and 1(c). The two-dimensional PhC based on the LN is arranged in a hexagonal array with a wedge angle of 60°. The red rods represent LN dielectric rods. The white background region represents air. The refractive index of the dielectric is $n = 2.143$. a is the lattice constant. r is the radius of the dielectric rod. Ports A and B are the two receivers that will measure the transmission of the incident light.

Figure 2 shows the map of the input light simulated by the finite-difference time-domain method. The incident light with a wavelength of 1.55 μm and an incident angle of 25° is composed of TE polarization and TM polarization with TE:TM = 1:1. After going through the PhC, the TE polarization is refracted in the negative direction, and is received by port A on the left side. The TM polarization is refracted in the positive direction, and is received by port B at the top side. Both of the transmissions are over 90%. This means that this PBS can realize the efficient and complete separation of TE polarization and TM polarization.

Here, we give the theoretical analysis of the PBGs of the PhC by using the plane wave expansion method, which needs at least two PBGs to achieve negative refraction. We assume that $2r/a = 0.6$ and plot the bandgap structure of the PhC as a function of the wave vector, as shown in Fig. 3. The negative refraction for the TE polarization

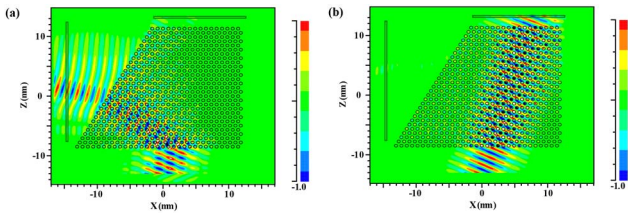

Fig. 2. Realization of the PBS. The incident light is separated after passing through the PhC. (a) TE polarization refracted in the negative direction. (b) TM polarization refracted in the positive direction. A and B are the two receivers to measure the light transmission.

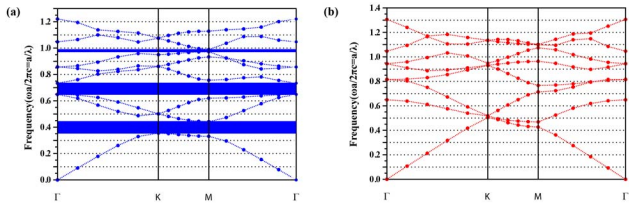

Fig. 3. Bandgap as a function of the wave vector for (a) TE polarization and (b) TM polarization.

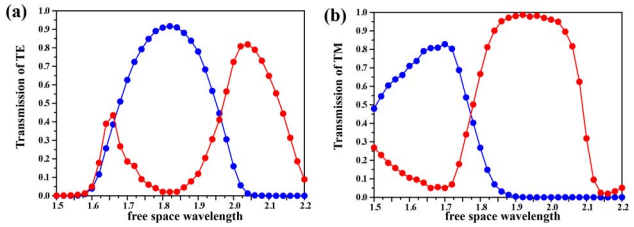

Fig. 4. Curves of transmission versus free-space wavelength based on the normalizing condition with the incident angle of 20° of the two polarizations. (a) TE polarization. (b) TM polarization. The optional free-space wavelength range based on the normalizing condition is 1.85–1.92 μm. The normalized frequency range is 0.52–0.54.

of the frequency occurs at 0.44–0.64 and 0.73–0.96. In this case, there is no PBG for TM polarization. Therefore, we can achieve the PBS under this condition.

Then, we study the relationship between the transmission and free-space wavelength based on the normalizing condition. Under this condition, the lattice constant and waveguide width are $a = 1$ μm and $2r = 0.6a = 0.6$ μm, respectively. The incident angle is 20°, and the transmission curves versus the free-space wavelength are shown in Fig. 4. The blue and red lines represent the received transmissions of the TE polarization (Fig. 4(a)) and the TM polarization (Fig. 4(b)) by ports A and B, respectively. When the free-space wavelength is 1.9 μm, port A receives the TE polarization and port B receives the TM polarization. Therefore, the incident light can be split into two directions with different polarizations, and the PhC acts as a PBS.

We choose the wavelength of 1.55 μm as the light source. According to the normalized frequency formula $f = \omega a/\pi c = a/\lambda$ (f is a constant), the parameters should be changed to: $a = 0.816$ μm, and $r = 244.8$ nm. Therefore, we change the free-space wavelength of 1.90 μm into the communication wavelength of 1.55 μm, based on the normalizing condition. The relationship between the transmission and incident angle is shown in Fig. 5. The blue and red lines represent the received transmissions by ports A and B. The solid and dashed curves represent the transmissions of the LN-based and the Si-based PBSs, respectively. Take the LN-based PBS for consideration: for TE (TM) polarization, the angle bandwidth range is 20°–30° (0°–28°) with a transmission of over 80% in port A (B). Therefore, the angle bandwidth range is 20°–28°

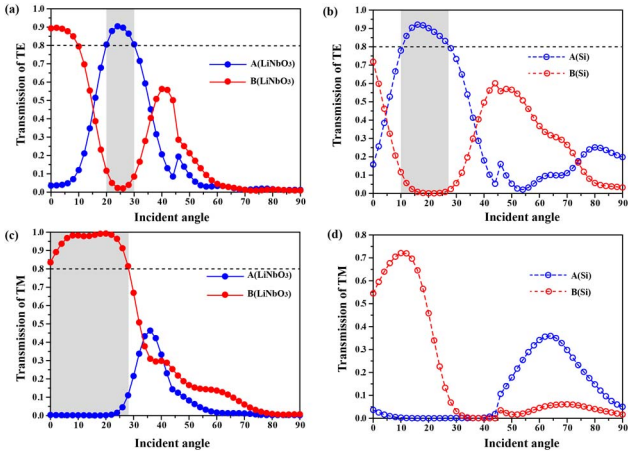

Fig. 5. Relationship between the transmission and incident angle. The gray segment represents the region where the PhC acts as a PBS. (a) TE polarization for LN-based PBS. (b) TE polarization for Si-based PBS. (c) TM polarization for LN-based PBS. (d) TM polarization for Si-based PBS. For the LN-based PBS, the angle bandwidth is 20°–28° with a light transmittance of over 80%. For the Si-based PBS, the transmission of TM polarization is less than 80%, due to the large reflection that occurs at the surface.

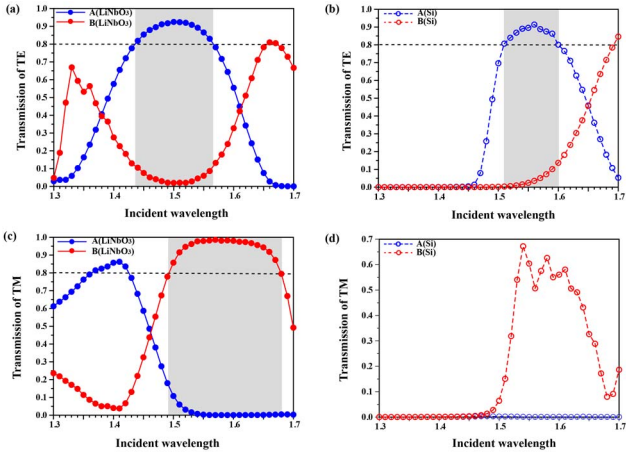

Fig. 6. Relationship between the transmission and wavelength. The gray segment represents the region that the PhC acts as a PBS. (a) TE polarization for LN-based PBS. (b) TE polarization for Si-based PBS. (c) TM polarization for LN-based PBS. (d) TM polarization for Si-based PBS. The wavelength bandwidth range is 1.50–1.57 μm, and the span of the wavelength is 70 nm with a transmission of over 80% for the LN-based PBS. The transmission of TM polarization based on Si cannot be over 70% under the condition of the two polarizations separating completely, because it has much more energy because of the surface reflection.

with a transmission of over 80%. But the transmission of the TM polarization is less than 80% for a Si-based PBS due to the large reflection that occurs at the surfaces. Therefore, the PBS based on Si has much more energy loss than LN. In conclusion, we can achieve a PBS with an angle bandwidth range of 20°–28° with an LN-based PBS.

Then, we choose 22° for the LN-based PBS and 14° for the Si-based PBS as the incident angles. The relationship between the transmission and wavelength is shown in Fig. 6. The solid and dashed curves represent the transmissions of the LN-based and the Si-based PBSs, respectively. Take the LN-based PBS for consideration: for TE (TM) polarization, the wavelength bandwidth range is 1.43–1.57 μm (1.50–1.68 μm) with a transmission of over 80% in port A (B). Therefore, the wavelength bandwidth range is 1.50–1.57 μm with a transmission of over 80%, and the span of the wavelength is 70 nm.

We compare the difference between the LN-based and Si-based PBSs. The transmission of TM polarization based on Si cannot be over 70% under the condition of the two polarizations separating completely. The LN-based PBS has a larger wavelength bandwidth than the Si-based PBS.

In conclusion, we demonstrate an LN-based PBS with a wedge-shaped negative refractive PhC. It has a good performance, including an efficient polarization splitting function with a high transmission of over 80%, an angle bandwidth of 8°, and a wavelength bandwidth of 70 nm. With a Si-based PhC, besides the large reflection that occurs at the surface and induces energy loss, no good PBS feature can be obtained with high efficiency. Combined with the other nonlinearities of LN, the LN-based PBS may play an important role in on-chip integrated quantum computation and quantum communication.

This work was supported by the National Natural Science Foundation of China under Grant Nos. 11574208 and 1174204.

References

1. R. C. Tyan, P. C. Sun, A. Scherer, and Y. Fainman, Opt. Lett. **21**, 761 (1996).
2. X. J. Yu and H. S. Kwok, J. Appl. Phys. **93**, 4407 (2003).
3. J. She, E. Forsberg, X. Y. Ao, and S. L. He, J. Opt. A: Pure Appl. Opt. **8**, 345 (2006).
4. M. Sesay, X. Jin, and Z. B. Ouyang, J. Opt. Soc. Am. B **30**, 2043 (2013).
5. T. Yu, H. J. Huang, N. Liu, J. Yang, Q. Liao, and X. Jiang, Appl. Opt. **49**, 2168 (2010).
6. C. Ren, J. Tian, S. Feng, H. H. Tao, Y. Z. Liu, K. Ren, Z. Y. Li, B. Y. Cheng, D. Z. Zhang, and H. F. Yang, Opt. Express **14**, 10014 (2006).
7. Y. Z. Liu, R. J. Liu, C. Z. Zhou, D. Z. Zhang, and Z. Y. Li, Opt. Express **16**, 21483 (2008).
8. L. Gan and Z. Y. Li, Sci China-Phys. Mech. Astron. **58**, 114203 (2015).
9. J. Lu, H. Ren, S. Guo, D. Gu, H. Wen, Y. Qin, S. Zhou, W. Hu, and C. Jiang, Chin. Opt. Lett. **12**, 102301 (2014).
10. A. M. Lerer, I. V. Donets, G. A. Kalinchenko, and P. V. Makhno, Photon. Res. **2**, 31 (2014).
11. Y. J. Zhang, Y. Wang, S. Y. Cai, M. Y. Lan, S. Yu, and W. Y. Gu, Photon. Res. **3**, 220 (2015).
12. X. Y. Ao and S. L. He, Opt. Lett. **30**, 2152 (2005).
13. Y. Ohtera, T. Sato, T. Kawashima, T. Tamamura, and S. Kawakami, Electron. Lett. **35**, 1271 (1999).
14. S. Kim, G. P. Nordin, J. Cai, and J. Jiang, Opt. Lett. **28**, 2384 (2003).

15. V. Zabelin, L. A. Dunbar, N. L. Thomas, and R. Houdre, Opt. Lett. **32**, 530 (2007).
16. M. Roussey, M. P. Bernal, N. Courjal, D. V. Labeke, F. I. Baida, and R. Salut, Appl. Phys. Lett. **89**, 241110 (2006).
17. G. Poberaj, H. Hu, W. Sohler, and P. Gunter, Laser Photonics Rev. **6**, 488 (2012).
18. G. Z. Li, Y. P. Chen, H. W. Jiang, Y. A. Liu, X. Liu, and X. F. Chen, Opt. Express **23**, 18345 (2015).
19. P. Hu, G. Li, J. Huo, Y. Zheng, and X. Chen, Chin. Opt. Lett. **13**, 121902 (2015).
20. G. Z. Li, Y. P. Chen, H. W. Jiang, and X. F. Chen, Photon. Res. **3**, 168 (2015).
21. M. J. Gong, Y. P. Chen, F. Lu, and X. F. Chen, Opt. Lett. **35**, 2672 (2010).
22. Y. Tang, Y. Chen, H. Jiang, W. Ji, Y. Wu, and X. Chen, Chin. Opt. Lett. **11**, 061901 (2013).
23. H. W. Jiang, Y. P. Chen, G. Z. Li, C. Y. Zhu, and X. F. Chen, Opt. Express **23**, 9784 (2015).
24. A. S. Solntsev, A. A. Sukhorukov, D. N. Neshev, and Y. S. Kivshar, Phys. Rev. Lett. **108**, 023601 (2012).